

**Project:** 1190

**Project title:** JPI Oceans / JPI Climate project ROADMAP

**Principal investigator:** Dr. Daniela Matei

**Allocation period:** 2022-01-01 to 2022-12-31

## **Achievements in 2022**

*Skilful prediction of the 2015 summer "cold blob" in the subpolar North Atlantic with the MPI-ESM1.2 "eddy-resolving" climate prediction system (K. Lohmann, O. Gutjahr, J. Jungclaus, D. Matei – manuscript in preparation)*

The subpolar North Atlantic is a hotspot with respect to predictability of sea surface temperature (SST) and upper-ocean heat content, as well as one of the regions worldwide, where initialisation with an observation-based state can further improve this predictability. Predictive skill of longer-term SST variability, such as the Atlantic Multidecadal Variability and the mid-1990s climate shift in the subpolar North Atlantic, is thoroughly discussed in the literature. Skilful prediction of high-frequency subpolar SST variability, in contrast, has not been demonstrated yet.

One impact-relevant SST event in the eastern subpolar North Atlantic is the record-cold anomaly in the summer of 2015, often referred to as "cold blob". It was largely driven by atmospheric forcing in the two preceding winters. A record-strong positive East Atlantic pattern (EAP) in the winter of 2013/14 and associated large heat loss to the atmosphere, led to a strong cold anomaly in the upper-ocean heat content. This preconditioning was maintained and further deepened by surface heat loss associated with a persistent, strongly positive North Atlantic Oscillation (NAO) in the winter and spring of 2014/15. A cold state of the subpolar North Atlantic has been identified as a precursor to the occurrence of European heat waves. Also the 2015 "cold blob" coincided with a major summer heat wave over central Europe. The ability to predict strong cold events in the subpolar North Atlantic is thus a topic of much interest.

In a first attempt to reforecast the 2015 summer "cold blob", Maroon et al. (2021) could not simulate the observed strength and extent in any of 60 prediction experiments initialized in November 2014 with the Community Earth System Model. They link this result mainly to the inability of their prediction experiments to reforecast the persistent, strongly positive phase of the NAO in the winter and spring of 2014/15. They suspect that prediction systems exhibiting higher skill regarding the NAO would be able to reforecast the 2015 summer "cold blob".

Here we analyse ensemble prediction experiments with the Max Planck Institute for Meteorology "eddy-resolving" climate prediction system to further assess the predictability of strength and extent of the 2015 summer "cold blob" in the subpolar North Atlantic. In contrast to Maroon et al. (2021), we initialize not only the ocean and sea ice, but also the atmosphere. Initial conditions of all three components seems crucial in simulating the 2015 record cold anomaly in the subpolar North Atlantic.

The "eddy-resolving" grid configuration, denoted as MPI-ESM-ER, shows reduced model biases compared to the MPI-ESM1.2 MPI-ESM-HR standard-resolution grid configuration ("eddy-permitting") applied in the sixth phase of the Coupled Model Intercomparison Project (CMIP6). Regarding the SST variability in the eastern subpolar North Atlantic, a key quantity of our study, the MPI-ESM-ER configuration exhibits both a realistic mean state and amplitude (Figure 1).

To assess the predictability of the 2015 record cold anomaly in the subpolar North Atlantic and the associated European heat wave, we have performed 20 prediction experiments initialized in November 2014 with an integration length of 26 months. Since the atmospheric forcing from the two preceding winters (winter 2014/15 and winter 2013/14) contributed to the subpolar cold anomaly, we have also performed 10 prediction experiments initialized in November 2013 with an integration length of 38 months.

In addition, we have performed a small set of multi-year prediction experiments covering the period 1992 to 2012, with initialisation dates in November every other year (three ensemble members with an integration length of 38 months each). The main purpose of these experiments is to bias-correct the prediction experiments initialized in 2013 and 2014. The additional prediction experiments also demonstrate that the MPI-ESM1.2 "eddy-resolving" climate prediction system is able to reforecast both the abrupt warming shift in the mid-1990s and the cooling trend in the 2010s in the subpolar North Atlantic (green lines in Figure 2).

To account for the different model and observation-based climatology as well as any model drift related to this difference, the prediction experiments initialized in 2013 and 2014 are bias-corrected prior to analysis. Bias-correction is done by subtracting, for each lead time, the mean of the respective lead time series constructed from the ensemble mean prediction experiments initialized between 1992 and 2012.

Though the observed record-cold anomaly in the subpolar North Atlantic in 2015 shows up also in the annual SST (black line in Figure 2), the absolute minimum occurred in the summer season with an average value of about  $-1.3^{\circ}\text{C}$  for the eastern part (black line in Figure 3). Regarding the spatial SST characteristics in the summer of 2015, cold anomalies are found in almost the entire subpolar region, with the exception of the Labrador Sea (upper panel in Figure 4). The strongest cooling occurred in the central eastern part with anomalies exceeding  $-2^{\circ}\text{C}$ . In the subtropical region, in contrast, warm anomalies are found, with the strongest warming located off the North American coast.

In contrast to Maroon et al. (2021), our prediction system is able to reforecast the cold anomaly in the subpolar North Atlantic in the summer of 2015. Individual ensemble members initialized both in November 2013 and November 2014 simulate the coldest SST anomaly in the summer season, with an average value in the eastern subpolar North Atlantic of about  $-1^{\circ}\text{C}$  (red lines in Figure 3). Furthermore, about 75% of the ensemble members (15 out of 20 members initialized in November 2014 and 7 out of 10 members initialized in November 2013) reforecast – on average – a cold SST anomaly in the eastern subpolar North Atlantic in the summer of 2015. Nearly all ensemble members initialized in November 2013 and November 2014 simulate an increase in eastern subpolar SST in 2016, thus a subpolar cold anomaly which peaks in 2015 (based on annual SST as reported last year for the first ten members initialized in 2014).

The area-average anomalies shown in Figure 3 are determined by both strength and spatial extent of the SST anomalies in the eastern subpolar North Atlantic. About half of the ensemble members initialized in November 2014 (9 out of 20 members) and one third of the ensemble members initialized in November 2013 (3 out of 10 members) reforecast cold conditions in the entire eastern subpolar North Atlantic in the summer of 2015, with maximum anomalies in the central eastern part reaching a similar magnitude as in observations (Figure 4 for the “coldest” member initialized in 2013 and 2014 respectively). Only exception is the warming in the region of the East Greenland Current in most of the ensemble members initialized in November 2014. Such a warming is not seen in observations. Most of the remaining ensemble members initialized in November 2013 and November 2014 reforecast cold SST anomalies at least in the central eastern subpolar North Atlantic, although of smaller magnitude compared to observations (not shown). Only three ensemble members simulate a warming in the entire eastern part. We note that the location of the maximum cold anomaly is shifted northward by about  $5^{\circ}$  latitude in our prediction experiments compared to observations (Figure 4). Even if not the focus of our study, we further note that most ensemble members initialized in November 2014 reproduce the warm anomalies off the North American coast. This warming is less clear in the ensemble members initialized in November 2013 (Figure 4 for the “coldest” member initialized in 2013 and 2014 respectively). Our next step will be to assess the mechanisms underlying the successful reforecast of the record-cold anomaly in the subpolar North Atlantic in the summer of 2015 as well as the spread of the subpolar SST anomalies among the ensemble members.

A cold state of the subpolar North Atlantic has been identified as a precursor to the occurrence of European heat waves. Also the 2015 "Cold Blob" coincided with a major summer heat wave over Europe (left upper panel in Figure 5). A preliminary analysis has shown that individual hindcast experiments could also successfully reforecast the large scale heat wave over Central to Southern Europe in the summer of 2015 (Figure 5, upper panel). Further analyses will investigate the connection between the 2015 “Cold Blob”, the formation of the high pressure ridge over Central Europe and heatwaves over Europe in the MPI-ESM-ER hindcast ensembles.

### *Reference*

E.A. Maroon, S.G. Yeager, G. Danabasoglu, and N.A. Rosenbloom. Was the 2015 North Atlantic subpolar cold anomaly predictable? *Journal of Climate*, 34:5403–5423, 2021.

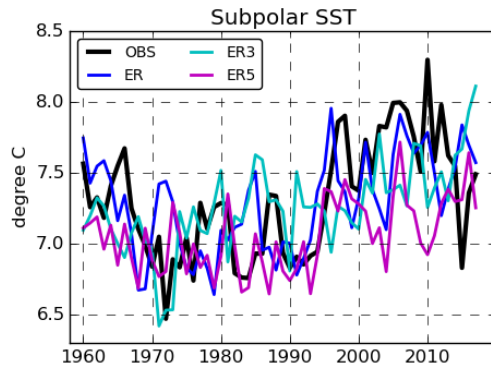


**Figure 1:** Annual SST ( $^{\circ}\text{C}$ ) in the subpolar North Atlantic (60W-15W, 50N-65N) in observations (black line) and in the three ocean-eddy-resolving historical simulations (coloured lines).

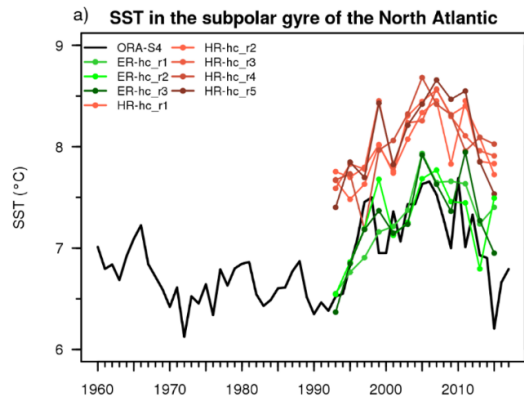


**Figure 2:** Annual SST ( $^{\circ}\text{C}$ ) in the subpolar North Atlantic (60W-15W, 50N-65N) in observations (black line), in the ocean-eddy-resolving prediction experiments (green lines, lead time 1 year) and in the CMIP6 prediction experiments (red lines, lead time 1 year).

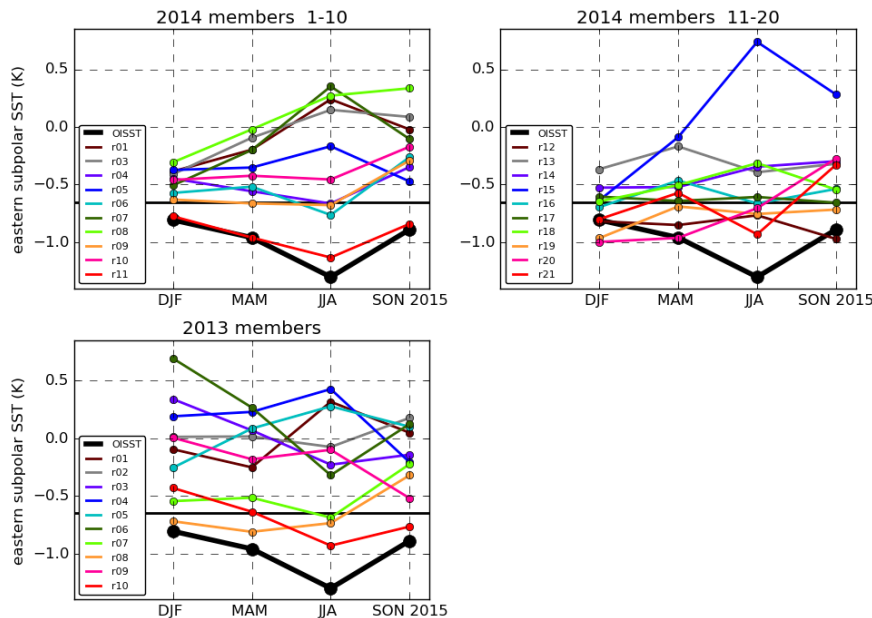


**Figure 3:** Seasonal SST anomalies ( $^{\circ}\text{C}$ ) in 2015 in the eastern subpolar North Atlantic (40W-15W, 50N-65N) in observations (black line, with respect to the mean over years 1993:2:2012) and in the bias-corrected prediction experiments (coloured lines) initialized in November 2014 (upper panels) and in November 2013 (lower panel).

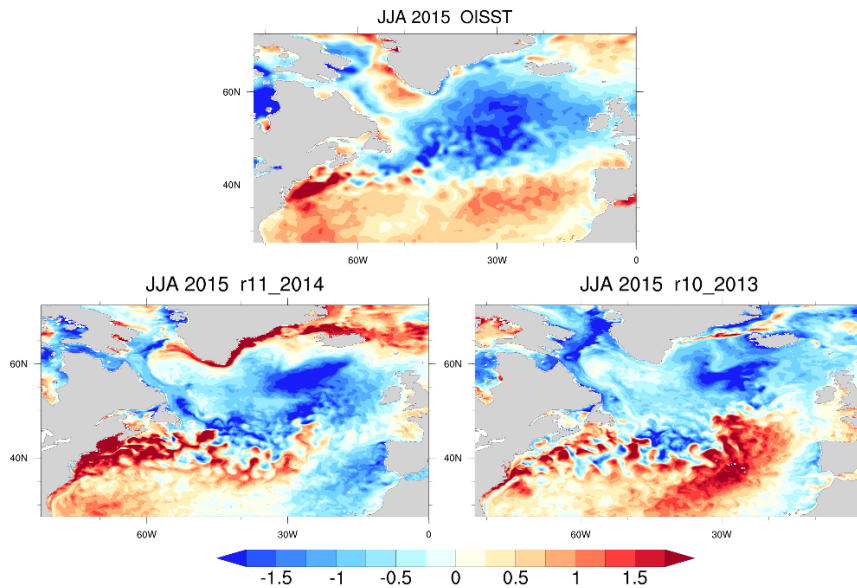


**Figure 4:** SST anomalies ( $^{\circ}\text{C}$ ) in the summer season (JJA) of 2015 in the North Atlantic in observations (upper panel, with respect to the mean over years 1993:2:2012) and in selected bias-corrected prediction experiments initialized in November 2014 (lower left panel) and in November 2013 (lower right panel).

### Predicted 2015 heat wave associated with high press. ridge over Europe

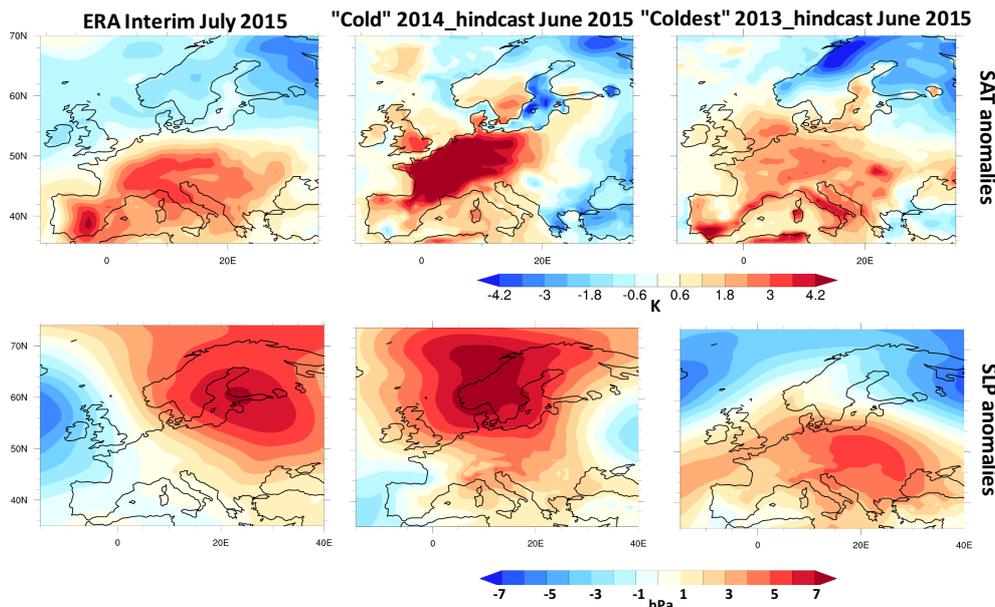


**Figure 5:** SAT anomalies ( $^{\circ}\text{C}$ ) in June 2015 over the European region in observations (upper left panel, with respect to the mean over years 1993:2:2012) and in selected bias-corrected prediction experiments initialized in November 2014 (upper middle panel) and in November 2013 (upper right panel), respective SLP anomalies (in hPa) in the bottom panel.

### Mid-latitude Atmosphere - Ocean interactions across scales

Linkages between modes of inter-annual variability in the sea surface temperature (SST) of the Pacific and Atlantic Oceans have been diagnosed making use of the Causal Effect Network method (CEN, Runge et al 2019) applied to outputs of the MPI-GE historical experiment. The MPI-GE historical experiment comprises an ensemble of 95 members of 155-year-long simulations. A comparable analysis has been performed with observed and reconstructed sea surface temperatures (HadISST, 1870-2021, Rayner et al 2003).

To explore the linkages between the Pacific and Atlantic Oceans we have defined four indicators of large-scale variability. These indicators are yearly time series of SST anomaly area averaged over specific regions, or principal component time series. For the Atlantic basin we have AMV\_ET, area averaged over (80W-0E, 30N-60N) and AMV\_TR, area averaged over (80W-0E, 0N-30N) time series. For the Pacific basin we have the PDV time series, which is the principal component of EOF1 for the region (120E-80W, 20N-60N), with positive phase defined for negative SSTA in the central North Pacific, and the EN34 (170W-120W, 5N-5S) time series, representing ENSO.

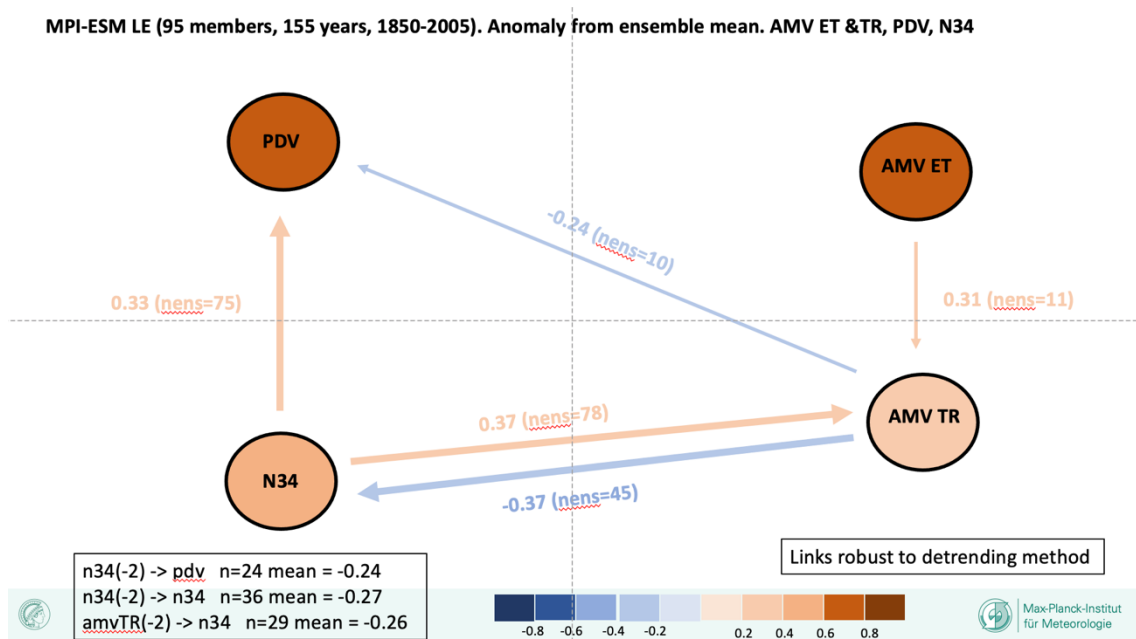


**Figure 6:** Causal effect network (CEN) showing the detected direct links between PDV, AMV\_ET, AMV\_TR, and N34 (the circles). Filling of the circles indicates autocorrelation at lag -1 year. Arrows depict links, -1 year lagged relationships. The color of the arrows shows the mean strength of the link, i.e., the value reported above the link. The mean strength is given by averaging over the statistically significant causal effect coefficients. The number of members with a significant statistically significant causal effect coefficient is reported in brackets.

Figure 6 shows the network of direct links between the four indicators. Significant links are found between most of the four indicators, in part confirming existing knowledge and in part posing questions to be addressed next. For instance, no direct link is found between the Pacific variability (PDV) and the extra-tropical Atlantic (AMV\_ET) and the latter appears to drive tropical variability only in a small number of members of the ensemble (i.e., 11 members). Here the open question is if a higher time resolution of the time series is necessary, to uncover potential links suggested in the literature. As expected, ENSO (N34) is an important source of variability, driving (leading) both PDV and AMV\_ET one year in advance, in a large number of members (nens=75 and 78 respectively). AMV\_ET as well is seen to lead both N34 and to a lesser extent PDV. Comparable linkages have been found for the observed and reconstructed HadISST, but for the N34 leads to the PDV, which in this case requires a seasonal time resolution. The comparison between HadISST and MPI-GE results provides for a novel evaluation of the modelled variability and will allow for estimating the contribution of midlatitude atmospheric dynamical processes to the connection between the Pacific and Atlantic Variability.

References:

Rayner, N. A.; Parker, D. E.; Horton, E. B.; Folland, C. K.; Alexander, L. V.; Rowell, D. P.; Kent, E. C.; Kaplan, A. (2003) Global analyses of sea surface temperature, sea ice, and night marine air temperature since the late nineteenth century J. Geophys. Res. Vol. 108, No. D14, 4407 10.1029/2002JD002670

Runge, J., P. Nowack, M. Kretschmer, S. Flaxman, D. Sejdinovic (2019) Detecting and quantifying causal associations in large nonlinear time series datasets. *Science Advances*. 5, eaau4996, <https://doi.org/10.1126/sciadv.aau4996>.

### Skilful decadal-scale prediction of fish habitat and distribution shifts

Many fish and marine organisms are responding to our planet’s changing climate by shifting their distribution. Such shifts can drive international conflicts and are highly problematic for the communities and businesses that depend on these living marine resources. Advances in climate prediction mean that in some regions the drivers of these shifts can be forecast up to a decade ahead, although forecasts of distribution shifts on this critical time-scale, while highly sought after by stakeholders, have yet to materialise. Here, we demonstrate the application of decadal-scale climate predictions to the habitat and distribution of marine fish species. We show statistically significant forecast skill of individual years that outperform baseline forecasts 3–10 years ahead; forecasts of multi-year averages perform even better, yielding correlation coefficients in excess of 0.90 in some cases. We also demonstrate that the habitat shifts underlying conflicts over Atlantic mackerel fishing rights could have been foreseen. Our results show that climate predictions can provide information of direct relevance to stakeholders on the decadal-scale. This tool will be critical in foreseeing, adapting to and coping with the challenges of a changing future climate, particularly in the most ocean-dependent nations and communities.

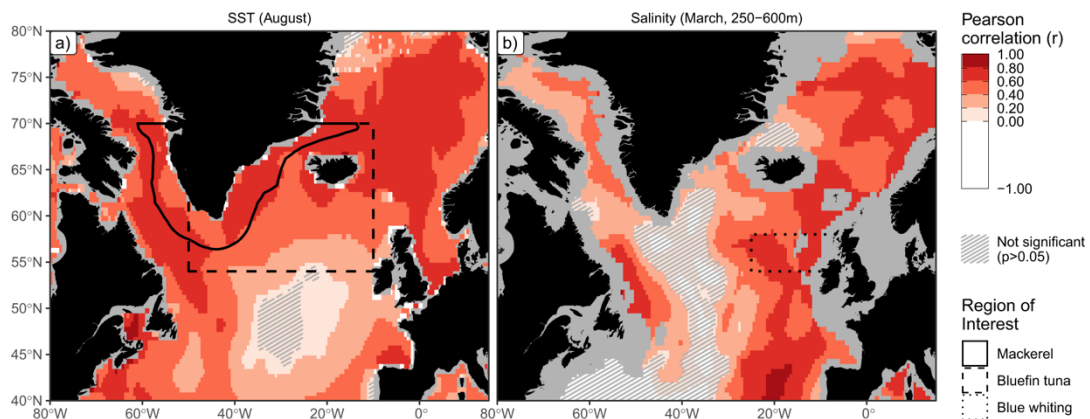


**Figure 7** Predictive skill of physical variables underlying our habitat forecasts from climate prediction systems with a lead time of five years for (a) mean August sea surface temperature (SST) and (b) mean March sub-surface (250–600 m) salinity. Predictive skill is expressed as the Pearson correlation coefficient ( $r$ ) between the forecast and observed values of each variable, with each grid point coloured according to the local value, evaluated over the period 1960–2018 for SST and 1985–2018 for salinity. Forecast skill is for the grand ensemble mean forecast, i.e., a forecast averaged across the individual realisations from all model systems. Regions where the correlation coefficient is not significantly greater than 0 (at the 95% confidence level, as estimated from bootstrapping) are cross-hatched. Lines mark the polygons over which the area of suitable habitat is calculated in subsequent analyses. Ocean regions not represented by all forecast models are shown in grey. From Payne et al., 2022.

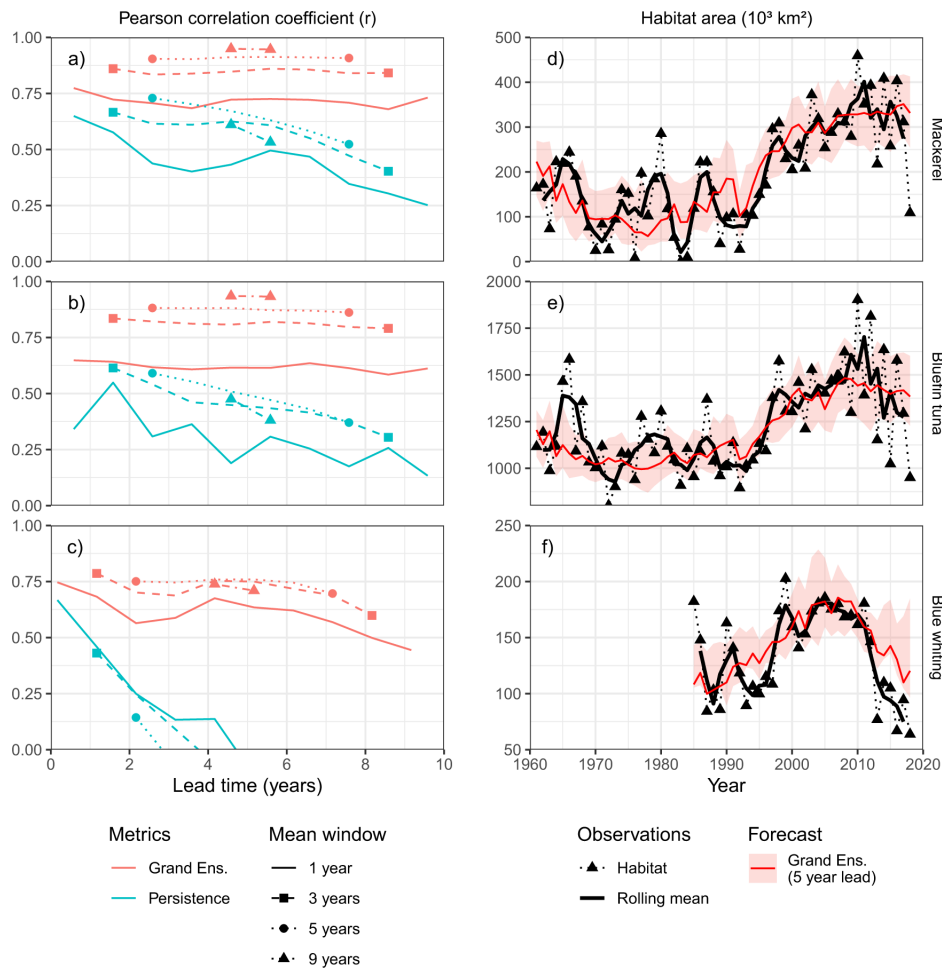


**Figure 8** The forecast skill of multi-annual averages of habitat area (panels a-c), as characterised by the Pearson correlation coefficient ( $r$ ), is shown for the grand-ensemble and persistence forecasts. In addition to the single-year values, the skill of multi-year averages (3, 5, and 9 year centred means) are also shown (broken lines with symbols). Lead-time is defined as the length of time from the issuing of the forecast (1 January) to the middle of the running mean window. Multiyear forecasts are significantly better than multiyear persistence for all lead times ( $p < 0.01$ , one-tailed test, as estimated by bootstrapping). Time-series of habitat metrics (panels d-f) show habitat estimates based on observations (triangles connected by dotted line) with their three-year running means (solid black lines). Habitat metrics forecast by the grand-ensemble (solid red line) with a 5-year lead time are shown with the corresponding 90% range of realizations (shaded area). Time series are shown for the full range of years used to estimate the forecast performance (i.e., 1961–2018 for mackerel and bluefin tuna, 1985–2018 for blue whiting). Panels (a) and (d) show results for the area of mackerel habitat around south Greenland, panels (b) and (e) bluefin tuna habitat south of Iceland, and (c) and (f) blue whiting spawning habitat west of Great Britain and Ireland. From Payne et al., 2022.

Reference:

M. Payne, G. Danabasoglu, N. Keenlyside, D. Matei, A. Miesner, S. Yang, S. Yeager, 2022: Skilful decadal-scale prediction of fish habitat and distribution shifts. *Nature Communications* 13 (1), 1-9.